SLAC-PUB-7948
September 1998

From CRID to DIRC*

J.Va'vra
Stanford Linear Accelerator Center, Stanford, CA 94309.

Abstract

The Barrel CRID detector has been operating successfully at SLD for the past seven years. It is an important tool for SLD physics analyses. The paper describes results based on long term operational experience of a number of important quantities such as the Cherenkov quality factor, N_0, of the device, fluid transparency, electron lifetime, single electron detection efficiency, anode wire ageing, TMAE purity, long term stability of the gas refraction index, liquid radiator transparency, Cherenkov angle resolution and the number of photoelectrons observed per ring. The DIRC detector is a novel particle identification detector to be used in the BaBar detector at SLAC. It is presently in its construction stage. The paper describes some of its most important R&D results.

I. INTRODUCTION TO CRID

The concept of the CRID at SLD (see Fig.1) benefited from the pioneering work of J. Seguinot and T. Ypsilantis [1]. The design is similar to that of the DELPHI RICH [2] and each group benefited from the work of the other. The early R&D developments of the Barrel CRID are summarized in Ref. 3, and its electrostatic design is described in Ref. 4. The detector main operating features and early CRID performance are described in Ref. 5. In addition, every year since 1986 we have presented some partial results at the IEEE conference. This paper summarizes our long term experience at a time when the SLD experiment is approaching the end of operation.

The CRID includes 40 TPC's, 40 liquid radiator trays containing liquid C_6F_{14}, a vessel containing a gas radiator composed of $87\%C_5F_{12}+13\%N_2$, and a system of 400 spherical mirrors [6]. The photoelectron drifts to a wire chamber where its position is reconstructed using a combination of drift time (z-coordinate), wire address (x-coordinate) and charge division (y-coordinate) with a precision of ~1x1x2 mm. The TPC gas is C_2H_6+TMAE (~0.1%). The maximum drift length is 1.2 m, and the maximum operating voltage is 55kV, which gives a drift field of 400 V/cm. The system operates at 35°C with the TMAE bubbler temperature set at 26-27°C, and has 3720 anode wires, 7440 amplifiers, 64000 field shaping electrodes and 6520 corona-preventing field wires.

During the initial stages of the CRID development we were concerned with possible problems such as: (a) breaking of 7μm dia. wires, (b) self-sustaining cathode currents (TMAE is an insulator), (c) wire ageing in TMAE (TMAE is a fragile molecule), (d) TMAE related disasters (broken pipe, leaky drift boxes), (e) single electron detection on such a large scale (~7440 channels), (f) 55kV HV and related problems (~65000 field wires), (g) wire ageing in TMAE (TMAE is a fragile molecule), electron lifetime in TMAE (can we maintain it?) (h) photon feedback (in core of jets), (k) coating of quartz by a pollution, (i) purity of fluorocarbons (we buy an ordinary industrial purity), (k) too much background from SLC, etc. At the end, the major issues we had to struggle with: (a) breaking of 7μm dia. wires (related to background. and possibly the Malter effect), (b) purity of fluorocarbons, (c) too much background from SLC (occasionally), (d) sulfur in ethane (this was a headache number #1), (e) contamination of optics in monochromators, etc.

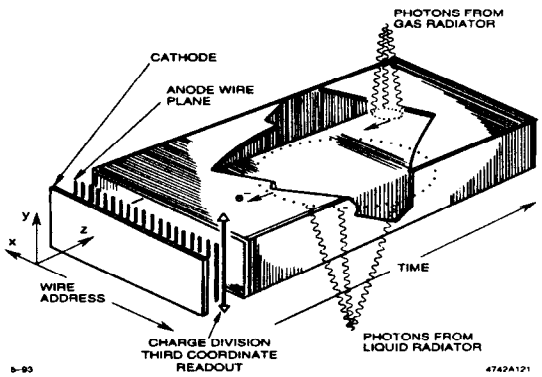

Figure 1. Principe of Cherenkov ring detection in CRID

II. CRID SYSTEM PERFORMANCE

A. *The Single Electron Detector*

1)General Performance

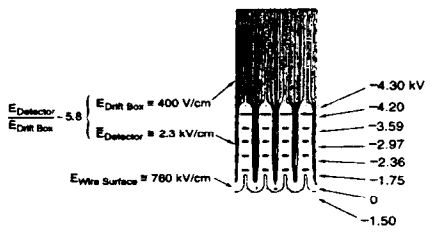

Figure 2. CRID single electron detector

*Invited talk at the Detector workshop, Jefferson National Laboratory, New Port News, Virginia, U.S.A., June 15-17, 1998. The work was supported by Department of Energy contract DE-AC03-765SF00515.

The single electron detector (see Fig.2) is based on single stage MWPC wire amplification with an average total gas gain ~$3x10^5$. The present CRID operating point corresponds to a single electron efficiency of about 85-90% [7]. To limit the avalanche photons entering the TPC drift volume, a system of Cu-Be blinds was constructed. The avalanche photons cause after-pulses. The measured rate of after-pulses per avalanche caused by the secondary avalanche photons is less than 1% at the operating point. The Cu-Be blind structure gives a factor of 7-8 reduction in the rate of after-pulsing. In order to have good electron transmission to the anode wire, the ratio of the drift field within the detector to that in the TPC is maintained at a value close to six. This makes the structure relatively insensitive to misalignments. The fact that the system of 3720 anode wires has been stable throughout seven years of TMAE operation demonstrates that the electrostatic design and the choice of operating conditions are sound.

2) Charge Division Performance

Initial experience and the very good charge division resolution (the resolution along the wire length), σ_z/ℓ~0.7%, obtained in early R&D tests [4,8], led to the choice of 7 μm carbon wire, even though such a thin wire is weak and difficult to handle. However, as a result of wire ageing arguments, the wire gas gain is set at as low a value as possible. This is the dominant factor in defining the observed charge division resolution, σ_z/ℓ~2.5% [9], which is nevertheless sufficient for the physics analysis (see Fig.3).

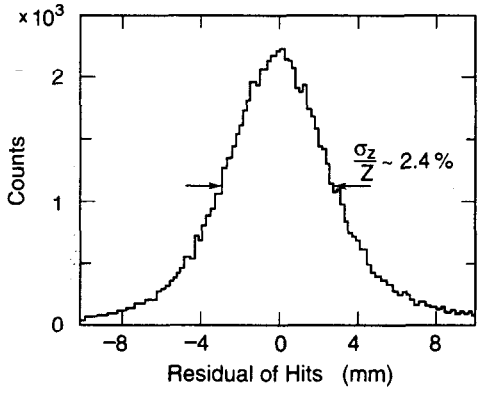

Figure 3. Charge division resolution using single photoelectrons in CRID detectors.

3) Wire Ageing

The TMAE molecule is very susceptible to polymerization. The prediction from the R&D ageing tests [10] is that a modest detector current of about 5-10nA would cause a 50% gain drop in about 1-2 years (see Fig.4). Figure 5(a) shows the wire ageing at SLD and indicates a decrease in gain of about 20-30% in a three year period; this result is consistent with the R&D data (a typical current 2-4nA per detector). From pulse height distribution measurements, we estimate that a 30% average gain decrease reduces the detection efficiency by about 5%. The rate of wire ageing was studied by monitoring the average single electron pulse height using UV fibers.

To regenerate the wire gain, we have shown in R&D tests that we can either wash the detectors with alcohol, or evaporate the deposits by passing a small (~10mA) current which heats the carbon wires to a temperature above 300°C. However, after ~7 years of running there is strong evidence that the wires have weakened to the point that they may be unable to tolerate this current without running a substantial risk of breakage. Tests with a detector which was removed from the SLD recently, indicate that such a procedure would be too risky. Therefore, the only option available is to clean the wires by washing the whole anode plane in ethanol. This was done to some detectors being repaired in the lab. Figure 5(b) indeed shows that there is an improvement in the relative average pulse height after such washing.

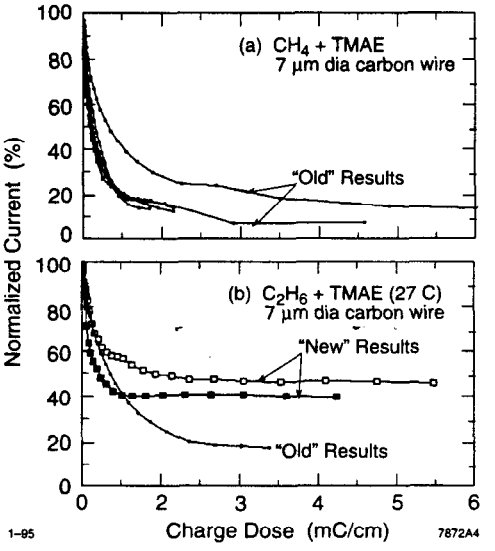

Figure 4. Wire ageing R&D results in (a) CH_4+TMAE, and (b) C_2H_6+TMAE gases [10].

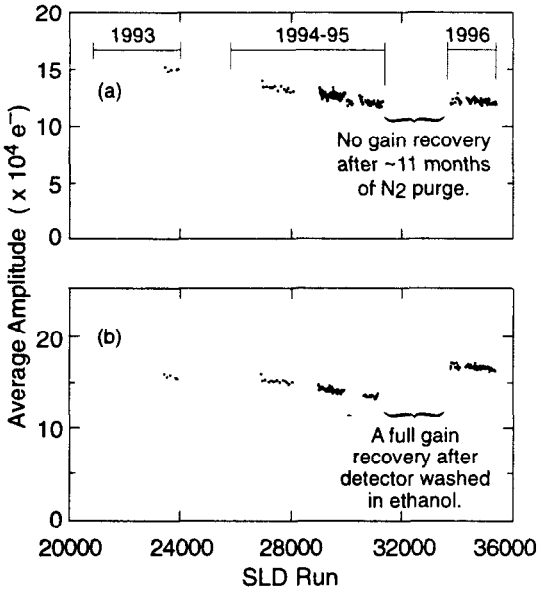

Figure 5. Wire ageing in the SLD CRID between 1993 and 1996 with: (a) a detector which was never removed, and (b) a detector which was removed after the 1995 run and washed in ethanol. The average pulse height is monitored using the UV fiber single photon calibration pulses [7].

4) Malter Effect

During the period from 1991 to 1993, our UV fiber trigger rate was set to the 120Hz SLC repetition rate. This caused local rates on some anode wires as high as 10Hz per cm of wire length. It was discovered [11] that this caused damage (probably in the form of an insulating film) to cathodes corresponding to wire locations aligned with the UV fiber fiducials. The damage would show up as a burst of charge every 15-20 minutes. Since then these wires cannot take a very high UV fiber rate. After the problem was discovered, the UV fiber trigger rate was reduced by a factor of 2000, and this yielded a reduction of the burst rate by more than a factor of 20. The total charge dose from the UV fiber source before the first bursts were discovered was estimated to be only about 2×10^{-7} C/cm, which is an exceedingly small amount. Of course, the subsequent burst charges increased the total charge dose rapidly. So far, during hadronic trigger running, this has not caused a problem due to sufficiently low charge density. However, it is obviously a concern for times when the SLC background is very large. A similar concern may come from background muons aligned with the TPC axis.

5) Wire Breaking

The 7 μm diameter carbon wires are definitely too fragile for the long term operation of such a large system as the CRID. They break at a rate of 3-5 per run, and this creates geometrical inefficiencies at a level of 5-10%. We try to repair detectors with broken wires during a run in order to minimize their impact. It is not clear why such breakage occurs, but we think it is due to material fatigue resulting from the total accumulated dose. This dose can be enhanced by excessive SLC noise during some periods (remember any single SLC pulse can create a very large background), due to background muons depositing charge axially in the TPC (> 10000 e^- per track), or due to the charge created by bursts related to the Malter effect. In retrospect, a choice of anode wire diameter between 20 and 33 μm diameter would have been better (wire ageing is also slower with thicker wire [10]).

B. Electronics Performance

We placed the amplifiers, analog storage (HAMU), ADC's and control and multiplexing circuitry on the detector [12]. Only a few serial optical fibers lead to the Fastbus located in the electronics control room. The amplifier charge gain is about ~2.7 μV/electron. To limit heating problems, amplifiers are water cooled, and all components except the first JFET use pulsed power. The analog storage needs to be calibrated every few days; the amplifier gain is calibrated once per run.

The amplifier-detector combination has cross-talk at a level of +1.1% for the first neighbor and about -0.25% for a distant neighbor [13]. This may seem small, but a typical charged track deposits about 1000 electrons in the TPC so that the cross-talk problem becomes significant. The amplifier recovery from such charge deposits creates spurious pulses, and also affects the measurement of real pulses. This is a complication for CRID analysis in the core of a jet, where many tracks overlap; for example, it causes a typical loss of 10-20% of the photoelectrons per liquid ring.

Any fault with the electronics located on the detector usually means that we have to wait for an SLD door opening in order to make repairs. Typically, we have ~1% dead electronics channels, randomly distributed at any given time during the run; from time to time some other larger segments fail, for example an ADC board, and this causes an additional ~1-2% dead channels, which tend to be clustered. However, it should be pointed out that it took several years before the electronics was debugged to this level. This is the price of placing complicated, inaccessible electronics on the face of the detector.

C. TPC Gas

The C_2H_6 gas[1] is cleaned in the standard way, i.e., we use mechanical filters,[2] Oxisorbs[3] and 13X molecular sieves.[4] In addition, we use electropolished stainless steel tubing, as is common practice in Silicon Valley industry (see Fig.6).

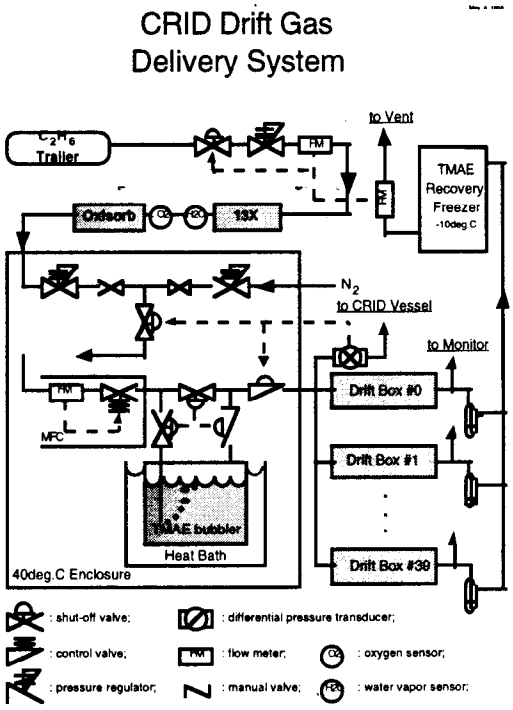

Figure 6. CRID TPC gas system.

We had serious problems with sulfur contamination. Our initial 1991 ethane supply was contaminated at a level of only 1-3 ppm, but that was sufficient to completely plug the ethane pressure regulator after one year of operation. The sulfur impurity level varies with the oil well which is the source of the ethane (as much as 200 ppm of sulfur has been reported). Sulfur can exist in ethane as elemental sulfur (dissolved in ethane liquid), CS_2, H_2S, SO_2 and COS. During the 1993

---

1 Purchased from AlphaGaz Co. with purity specification: 99.995%.

2 Mechanical Waferguard filter, 0.05 micron, Milipore Co., U.S.A.

3 Oxisorb made by Messer Griesheim GmbH, 4000 Dusseldorf, Germany.

4 13X Molecular Sieve made by Union Carbide Co., Danburg, CT 06817-0001, U.S.A.

physics run we tried using a nickel getter[5] to remove this contaminant. This caused day-to-night variations in drift velocity, which could not be corrected by means of a simple pressure and temperature correction. Instead, we had to rely on the UV fiber drift velocity off-line calibrations. There was also a small release of oxygen from the nickel getter over a period of time, which prompted us to introduce another Oxisorb cartridge on the gas pad. This experience illustrates that some very active substances used in modern cleaning filters, such as nickel, can give rise to very complicated chemistry. As a result, in 1994, we decided to buy sulfur-free ethane in Europe. The sulfur level was specified to be less than 1ppm. The 1994 and 1995 physics runs went without any problem. However, in the 1996 and 1997 runs the same plug-up problems developed despite very tight sulfur specifications. For example, we see elemental sulfur deposits in the gas regulator (see Fig. 7), and we also clearly recognize the characteristic smell of SO_2. This indicates that the gas company's certification documents cannot be trusted. Each gas delivery must be checked independently. It was sulfur, and not TMAE, which was the biggest source of grief for long term operation of the CRID.

The TMAE[6] is cleaned by the CRID group by (a) washing it with oxygen-free deionized water, (b) filtering through silica gel and 3A and 4A molecular sieves, and (c) pumping [14] it at elevated temperature (~60°C) and at a pressure of a few Torr for 12-24 hours.

This operation was perfected over many years, and resulted in the production of TMAE of consistently good quality by removing various contaminants, such as TMO, which is soluble in water (it has a ~40x times higher electron capture rate than oxygen [15]). Before the TMAE is used in the TPC's, it is qualified in a small ionization chamber (ELM) [16]. Figure 8 shows an example of electron lifetime after TMAE washing with two different bubblers before use in the 1997-98 physics run. One can see a clear improvement in TMAE purity when pumping is used compared to simple filtering. When the TMAE washing is finished, the electron lifetime is almost the same in the TMAE laden gas as in the carrier gas, in this case CH_4 [7].

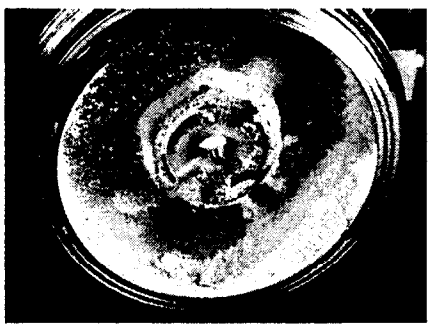

Figure 7. Sulfur deposits in the ethane gas pressure regulator.

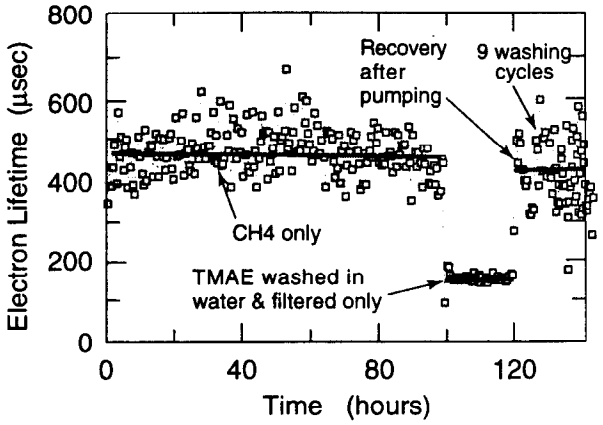

Figure 8. TMAE washing: (a) measured electron lifetime with CH_4 only, (b) with CH_4+TMAE where TMAE was just washed in water and filtered, (c) as (b) but also pumped for 12-24 hours at a pressure of a few Torr at 60°C [7].

D. Gas Radiator

Our gas radiator recirculation system operates as a heat engine (see Fig.9). We believe that the simple distillation and condensation cycle in our heat engine recirculation system helps maintain the required purity of the radiator gas. The returning gas mix from the vessel enters a -90°C tank where the C_5F_{12} liquefies, and the N_2 gas is vented; this also serves to remove some gaseous impurities. The C_5F_{12} liquid is then evaporated again and mixed with new N_2 gas. The overall flow generates one complete volume change every 10-11 hours. In parallel, the C_5F_{12} liquid is circulated through a system of silica gel,[7] elemental copper (RIDOX),[8] and Oxisorb filters. The idea is that the silica gel protects the other filters.[9] We do not regenerate any of these cartridges for fear of possible dissociation of C_5F_{12} molecules during the heating process.

We monitor the radiator transmission using two methods: (a) we pump a return gas mixture from the vessel to a gas rack monochromator, where it is measured in a 20 cm long UV cell, or, (b) we take a liquid C_5F_{12} sample from the -80°C tank directly into either a 1cm thick UV cell or a small glass bottle, and then take this liquid to another monochromator. Figure 10 shows that the measurement of the 87%C_5F_{12}+13%N_2 gaseous sample using the 20 cm long cell is consistent with that using the 1 cm thick liquid sample, after both have been scaled to the average photon path length 67.5 cm. Both CRID measurements are only slightly worse than the results from the DELPHI 1cm thick liquid sample, which was obtained by fractional distillation [17]. This indicates that the results of our C_5F_{12} purification procedure are nearly the same as those obtained by the DELPHI group. Figure 11 shows good

[5] Nickel catalyst N1-0104T-1/8 made by Engelhard Co., Iselin, NJ 08830-0770, U.S.A.

[6] TMAE stands for Tetrakis dimethylamino ethylene, and was purchased from RSA Co., U.S.A.

[7] Silica Gel Sorbead R was purchased from Adcoa Co., Gardena, CA 90247, U.S.A.

[8] Elemental Copper is made by Engelhard Co., Elyria, OH 44035, U.S.A. (The process is called Q-5.)

[9] The procedure recommended to us by 3M Co., St. Paul, Minn. 55144-1000, U.S.A.

reproducibility of the transmission measurements using liquid samples from the -80°C tank, taken during different periods.

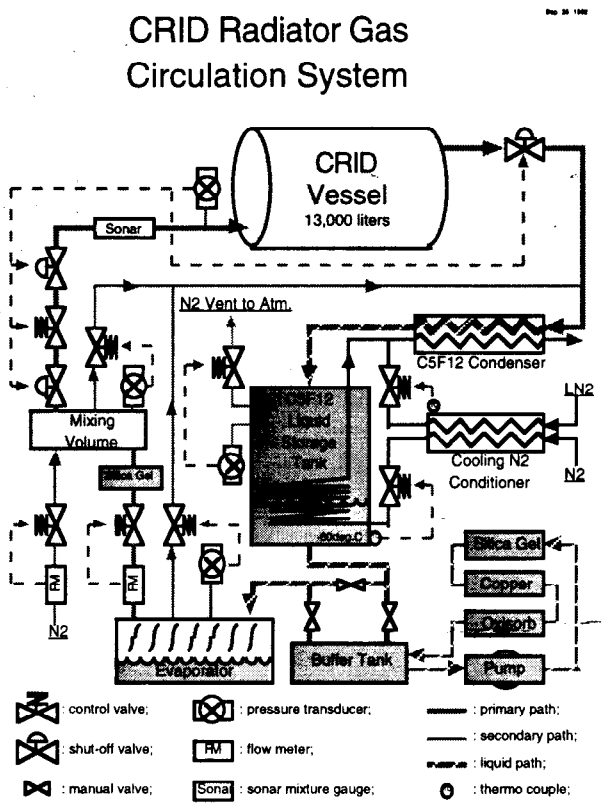

Figure 9. Gas radiator purification system

Any instability in the $87\%C_5F_{12}+13\%N_2$ mix causes instability in the refractive index, and thus the Cherenkov angle. The gas radiator mixture in the vessel is continuously monitored by sonar [18] - see Fig.12.

The data are then used in the off-line analysis. Figure 13 shows the time history of the Cherenkov angles in this radiator obtained from off-line reconstruction, in comparison to the angles obtained from the sonar measurements. The agreement is very good. Therefore, sonar can be used to correct the data during periods when we do not have high statistics in Z^o events. The mix stability improved in the 1996 data because we have started to control the mix with the on-line sonar hardware information.

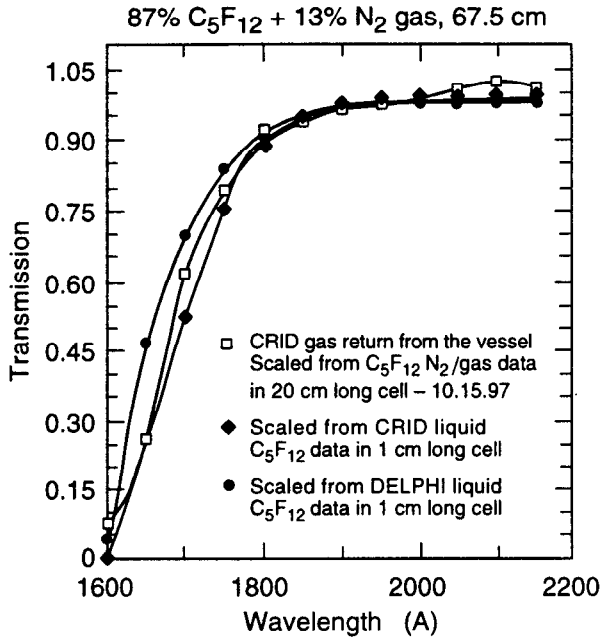

Figure 10. The transmission of C_5F_{12}/N_2 gas, taken from the vessel return and measured in a 20 cm long cell, compared to liquid measurements properly scaled [7].

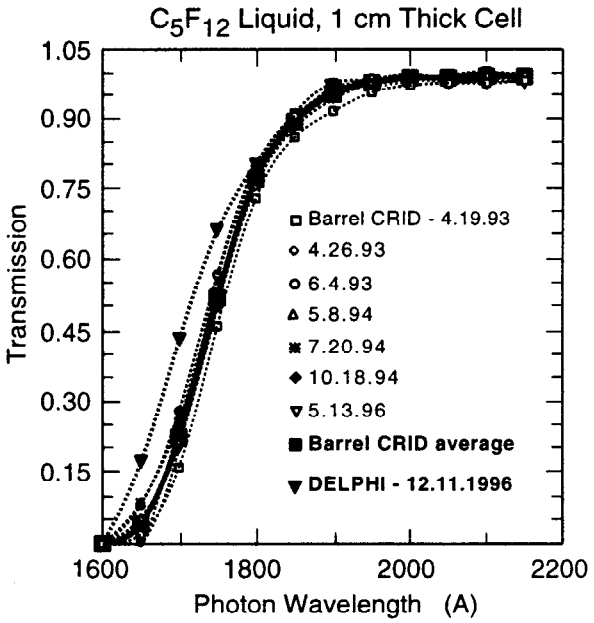

Figure 11. The transmission of C_5F_{12} liquid taken from the -80°C tank and measured in a 1cm thick cell. Six SLD measurements from different periods, and their average, are compared to the current DELPHI results [7].

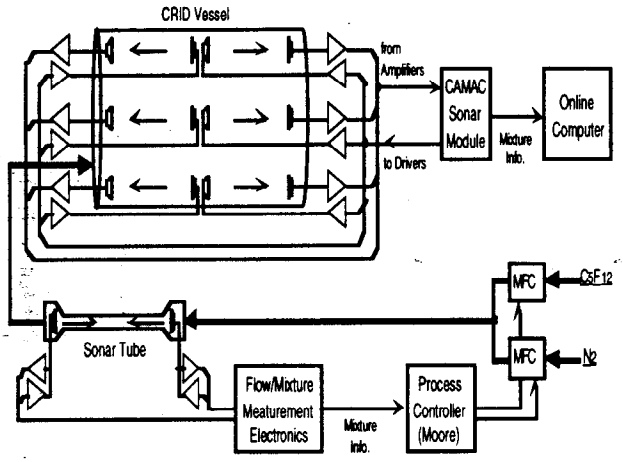

Figure 12. CRID Sonar system in the gas radiator vessel.

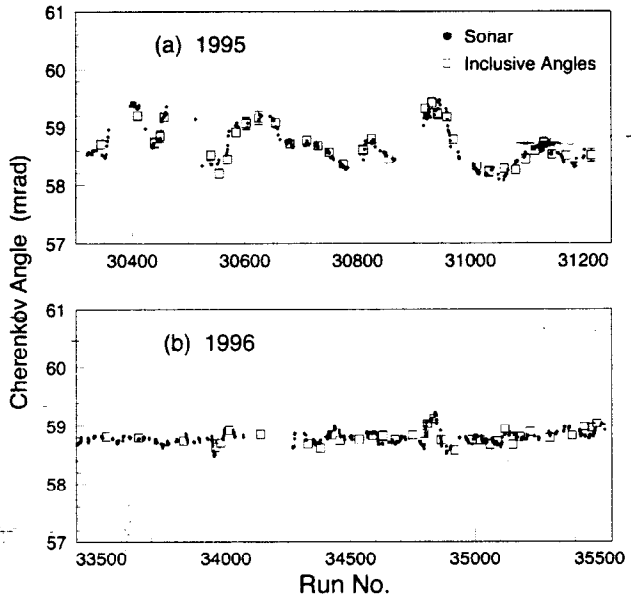

Figure 13. The $\beta \sim 1$ Cherenkov angle measured from ring reconstruction (squares) compared to the value expected from the gas index measured by sound velocity in the CRID vessel and corrected for atmospheric pressure (dots).

E. Liquid Radiator

The C_6F_{14} liquid is initially de-oxygenated and purified by bubbling N_2 gas through it (see Fig.14). During the run, the liquid is purified by pumping it through Oxisorb. The recirculation flow is one radiator volume very two hours. The Oxisorb is changed every three months. In this system the Oxisorb is not protected by silica gel. However, we do know that the 3M company uses silica gel to clean the liquid before shipping, and our experience to date is satisfactory. We have never experienced problems with improperly fluorinated C_6F_{14} molecules such as those experienced by the DELPHI group

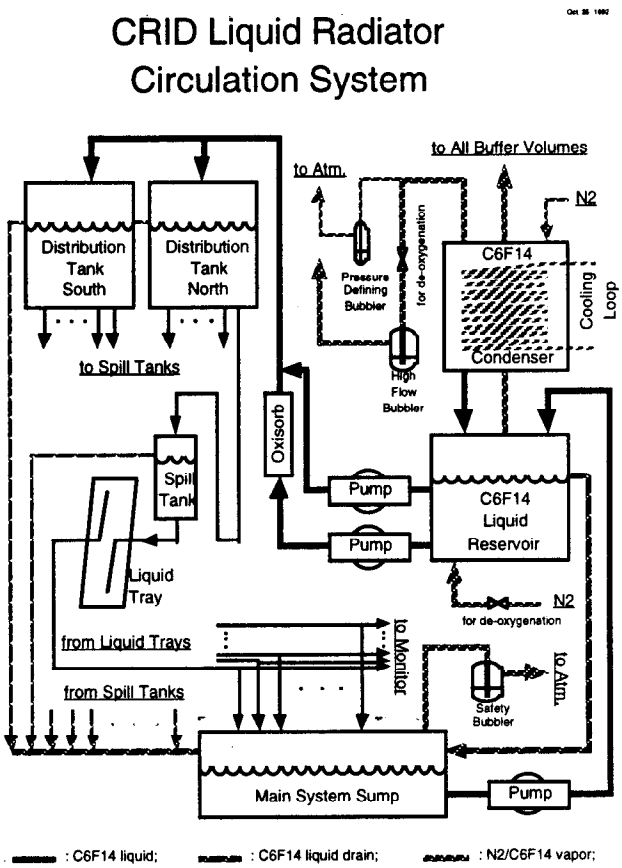

Figure 14. CRID liquid radiator system.

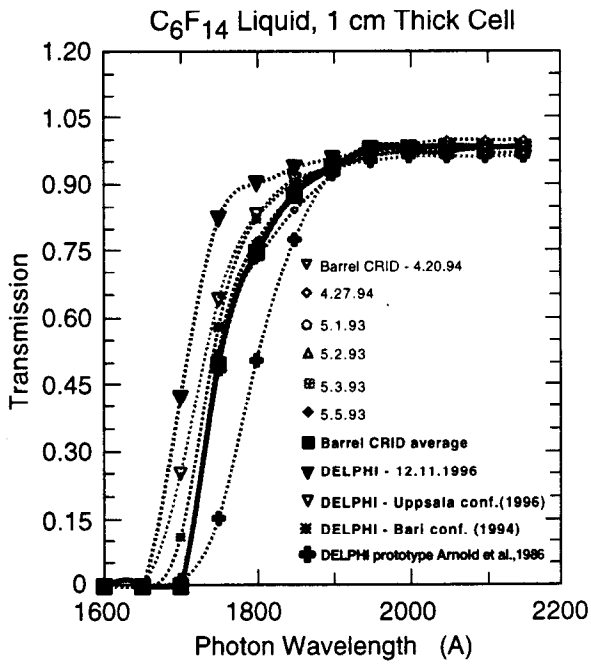

Figure 15. The transmission of C_6F_{14} liquid measured in a 1cm thick cell. Six SLD measurements from different periods, and their average, are compared to the current DELPHI and older DELPHI prototype results [7].

[17,19], which caused severe transmission problems in the early period of their running. However, Fig. 13 shows that our simple filtering method is not equivalent to cleaning by fractional distillation, which DELPHI presently uses to separate C_5F_{12} and C_6F_{14} molecules, because of leaks between the liquid system and the gas radiator. Figure 15 also shows that by the time of the Bari RICH conference both experiments had similar transmission; at that time DELPHI did not yet use the distillation process. After the process was introduced one can see a steady improvement. One can also see that the early DELPHI prototype from 1986 had even worse C_5F_{12} transmission. We were interested in testing whether the transmission might be improved by a different kind of filtering. Figure 16 shows an attempt to take the liquid from the CRID system and pass it once through an Oxisorb, or Silica gel, or RIDOX filter. It is interesting to note that silica gel is equivalent to Oxisorb; on the other hand, RIDOX filtering is worse. This indicates that our purity could be improved if we increased our filter capacity substantially, at least in principle. However, probably the best way to clean the commercially available C_5F_{12} or C_6F_{14} molecules is to distill them.

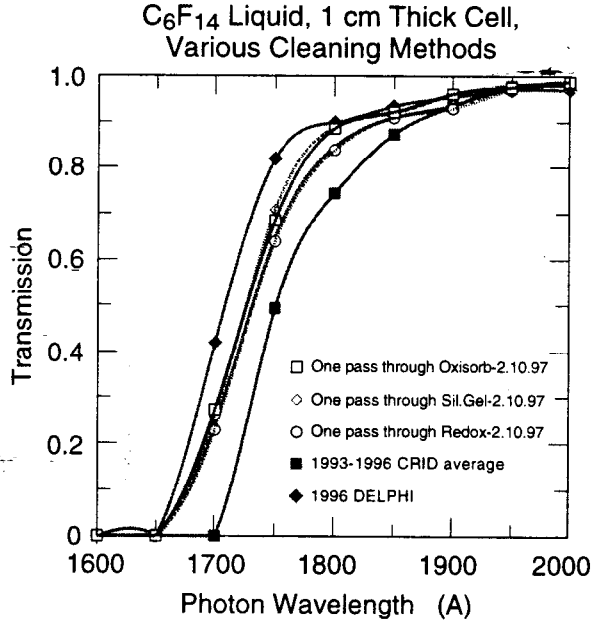

Figure 16. Attempt to take the liquid from the CRID system and pass it once through an Oxisorb, or Silica gel, or RIDOX [7].

F. High Voltage

In the early days we worried that any corona on field wires might cause a very large photon background in nearby TPCs. This did not occur, mainly because of our conservative design for the electric gradient on the field cage wires (<20 kV/cm). To define the drift field in the TPC's, we decided to use a simple geometry for the field cage wires rather than a volume degrader. Our experience with high voltage is excellent indicating that it is not necessary to build a volume degrader for voltages up to 60 kV and distances of 8-10 cm to ground, provided that a gas with good dielectric properties fills the volume.

We had good experience with all high voltage cables used both for the 55 kV TPC operation (inside the radiator vessel we use ~3 m long 100 kV Belden polyethylene cable, outside we use ~30 m long 125 kV silicone Alden cable) and for the 1.5-5 kV MWPC detector operation (in this case, we use ~30 m long 10 kV Belden polyethylene cables), and also with all power supplies made by the CAEN and Gamma H.V. Research companies. We had good experience also with thin film resistors used for TPC field grading and spark gaps used to protect them in case of a spark.

G. Material Stability

1) Materials Exposed to TMAE

Generally, all materials exposed to TMAE are in excellent shape after ~7 years of SLD operation and 10 years after the initial construction. This includes hard epoxies (DP-190 or Epon826+Versamid140), Cu-Be electrodes of the detector (they are as shiny as new), Viton O-rings[10] used to seal the MWPC detector to the TPC (in the early days we worried about the longevity of such a soft material in TMAE), TMAE bubblers, etc. This comes from visual inspection of both TPCs and the MWPC detectors, and also from the fact that the oxygen level in the return gas from all TPC's is the same as seven years ago, i.e., below 1ppm. Perhaps the only weak part of the entire system exposed to TMAE is the Alodined plating of an aluminum surface within the MWPC detector and the TPC detector enclosure; this plating seems to come off relatively easily when rubbed with a Q-tip dipped in ethanol.

2) Materials Exposed to C_5F_{12}

We see clear signs that this particular molecule, which is a solvent, leaches a small amount of plasticizer from the RF gasket[11] used to seal the radiator vessels' sector covers. The plasticizer is deposited on the clamps located a few mm away. However, because we keep a slight positive pressure in the vessel (~0.5Torr), this effect is believed not to be harmful to sensitive components within the vessel.

3) Materials Exposed to C_6F_{14}

We do not see any obvious deterioration. In the early period of CRID running we have seen pollution leaching from the DP-190 epoxy into the C_6F_{14} liquid, thereby affecting the UV transparency. To solve this problem, it was found necessary to circulate C_6F_{14} liquid continuously and filter out this pollution using an Oxisorb filter.

However, based on our lab tests, the liquid trays, which were built using G-10 panels and quartz windows, do change shape under gravity; it is possible that this effect results in poorer angular resolution than expected for Cherenkov rings in the liquid (we have to add ~10 mrad in quadrature with the resolution obtained in Monte Carlo simulation to reproduce the data).

H. *CRID Monitoring*

There are several levels at which the CRID system is monitored: (a) the absolutely critical variables, such as TPC or

[10] Viton O-ring, Parker Co., Part number : VO747-75, Cure 4Q87.

[11] "Elastomet" rubber gasket filled with 5056 aluminum wire made by Nova-tronix Inc., Santa Clara, CA 95054, U.S.A.

gas radiator pressure, are tied to an automatic hardware control which protects the basic integrity of the system by switching off the gas flow [20]; (b) a very important part of the safety system is the SIAM alarm system, which allows monitoring of about 80 variables; some critical variables are connected to an auto-dial paging system, and some can cause an automatic TMAE bubbler bypass; without the SIAM system the CRID would not have been successful; (c) another important feature of the CRID is slow self-monitoring of each TPC by measuring, for example, the Cherenkov angle distribution at the end of each 4 hour running period [see Figs. 17(a) and 17(b)], the average TPC z-coordinate formed from single electron pulses plotted as a function of time, the average number of hits per gas or liquid Cherenkov ring, etc.; in a way, this is the final arbiter of performance; (d) in addition, there is an extensive on-line monitoring system [21] which gives quantities such as the electron lifetime in selected TPCs, the mix ratio in the radiator vessel based on sonar, various averages, etc.

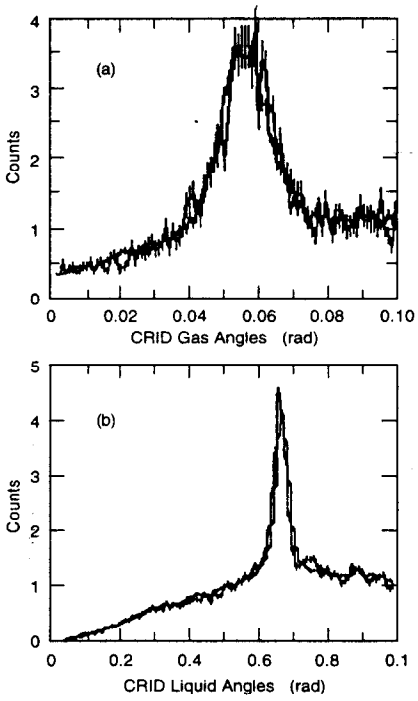

Figure 17. (a)-(b) On-line monitoring of the Cherenkov angles at the end of each run (~4 hour running period).

I. Simple Estimate of N_o

It is useful to define a "starting efficiency," which can then serve as a limit on how well one can do in the best possible circumstance. It is limited only by the TMAE quantum efficiency and basic material transmissions. For liquid rings, the "starting efficiency" is defined by the wavelength dependent transmission through quartz, $T_{quartz}(E)$ [corrected for photon path length 4mm/cos(38.5°); and applied twice], C_6F_{14} liquid, $T_{C_6F_{14}}(E)$ [corrected for photon path length 1cm/cos(38.5°)], and the TMAE quantum efficiency, $\varepsilon_{TMAE\,QE}(E)$. For gas rings, the "starting efficiency" is defined by the transmission through the quartz window, $T_{quartz}(E)$ [assume 4mm photon path length; applied once], 87%C_5F_{12}+13%N_2 gas, $T_{C_5F_{12}/N_2}(E)$ [corrected for ~67.5cm photon path length ~1.5*45cm], the mirror reflectivity, $R_{mirror}(E)$, and the TMAE quantum efficiency, $\varepsilon_{TMAE\,QE}(E)$. There are many corrections which degrade the "starting efficiency." They are derived from a collection of efficiencies, such as those measured during the construction period (transmission of quartz, mirror reflectivity, and TMAE quantum efficiency [22]), and those measured during the run (MWPC chamber efficiency UV transmission of fluorocarbons, oxygen, and water effects), together with estimates of other factors, such as absorption by the field cage wires, electron lifetime, TPC gaps, TMAE absorption length, etc. We call the degraded efficiency a "final efficiency." The "starting" and "final" efficiencies are shown in Figs. 18 and 19, and Table 1 lists estimates of the total degradation factors between the "starting efficiency" and the "final efficiency". For more detailed discussion of the Barrel CRID efficiencies and degradation factors see Ref. 7.

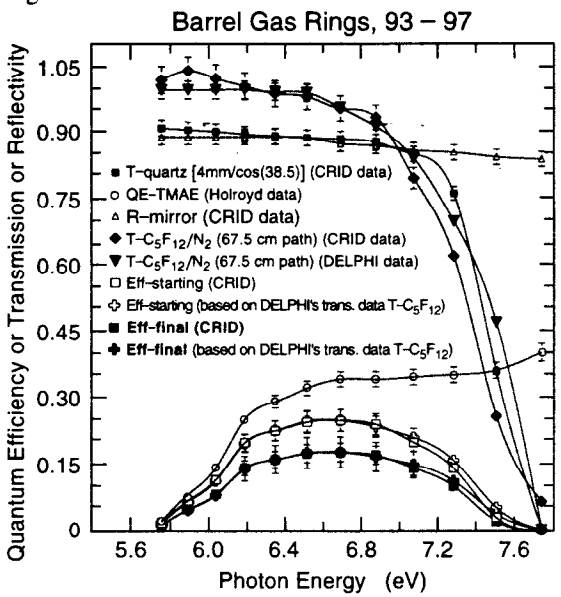

Figure 18. Barrel CRID gas rings with the C_5F_{12}/N_2 radiator: transmissions for quartz (4mm) and the 87%C_5F_{12}+13%N_2 gas radiator [for an average photon length ~1.5x45 cm], reflectivity of mirrors, TMAE quantum efficiency (Holroyd), and the "starting" and "final" efficiencies [7].

The above mentioned method does not include effects such as those due to the confusion in the middle of jets (the cross-talk and amplifier recovery cleaning cuts, and small electron losses due to the Lorentz angle in the liquid rings). Therefore, it is expected to be useful only for simple events, such as di-muons, where we observe 16-17 photoelectrons per full liquid ring, and ~10 per gas ring; this is consistent with the simple calculation at the level of 10%. Notice that we could increase the total number of photoelectrons per liquid ring by 2-3 if we were to achieve DELPHI's C_6F_{14} purity, which was obtained by fractional distillation instead of filtration.

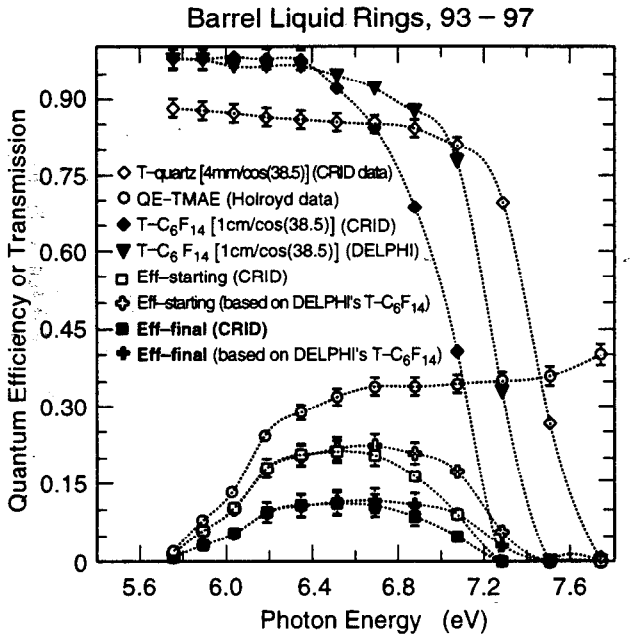

Figure 19. Barrel CRID liquid rings: transmission for quartz (4mm) and the C_6F_{14} liquid radiator (1cm), TMAE quantum efficiency (Holroyd), and the "starting" and "final" efficiencies [7].

Table 1. CRID final performance for gas and liquid rings

Parameter	Gas Rings	Liquid Rings
Total fraction of photoelectrons contributing to the "final efficiency" compared to the "starting efficiency" Eff_{final} / $Eff_{starting}$	0.70	0.53
Mean photon energy [eV]	6.70	6.50
Mean refractive index	1.001646	1.27202
Mean Cherenkov angle [mrad] (β=1 particle)	57.33	666.24
Calculated for radiator length [cm]	45	1
N_0 [cm^{-1}]	80	42
Expected average number of photoelectrons per full ring (β=1 particle) [7]	11-12	16
Measured average number of photoelectrons per full ring (di-muons) [21]	10	16-17

III. CRID RESULTS AT SLD

Figure 20(a) shows the Cherenkov gas ring angular resolution for di-muons [21]. This particular resolution is obtained by making circle fits to gas rings, and represents the "internal resolution" (3.6mrad) of the CRID; it indicates that the TPCs are reconstructing data with a resolution close to design value. Figure 20(b) shows the same for full liquid rings close to a 0° dip angle. The expected resolution is about 12mrad. This means that we have to add about ~10mrad in quadrature to explain the data; this ~10mrad represents systematic errors due to misalignments, for example, distortions in liquid trays.

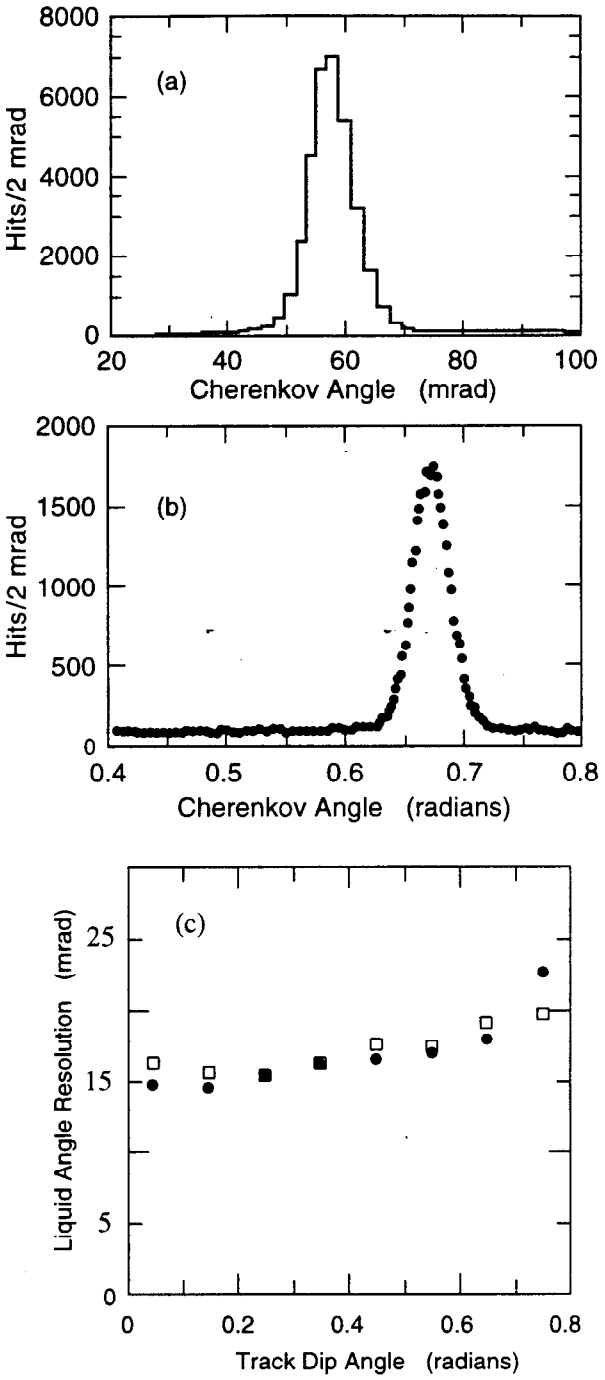

Figure 20. Cherenkov angle resolution in $e^+e^- \to \mu^+\mu^-$ events for: (a) gas rings (~3.6mrad; residuals from the fitted circle to show the internal TPC resolution), (b) liquid rings (~15mrad; inclusive resolution) at 0^o dip angle, and (c) liquid rings as a function of dip angle (squares are from hadronic events, while dots are from $e^+e^- \to \mu^+\mu^-$ and $e^+e^- \to e^+e^-$ events) [21].

Figure 20(c) shows this resolution as a function of dip angle. We see about 10 photoelectrons per gas ring, and 16-17

photoelectrons per liquid ring for di-muons [21], i.e., close to expectation for simple events—see Table 1.

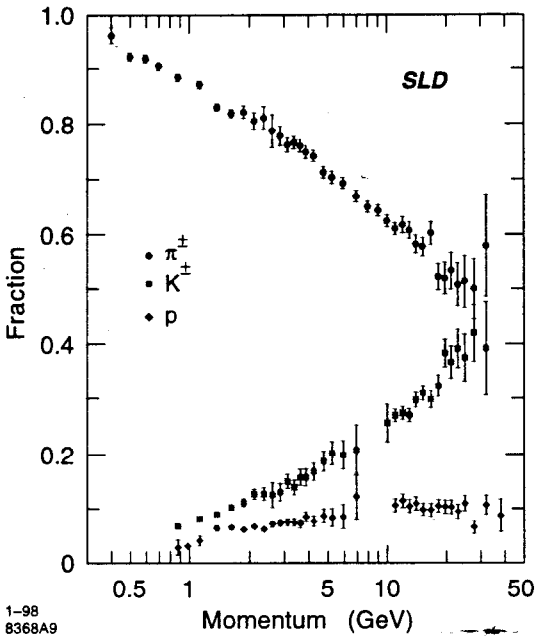

Figure 21. Particle fractions from Z^0 decays as a function of momentum [23].

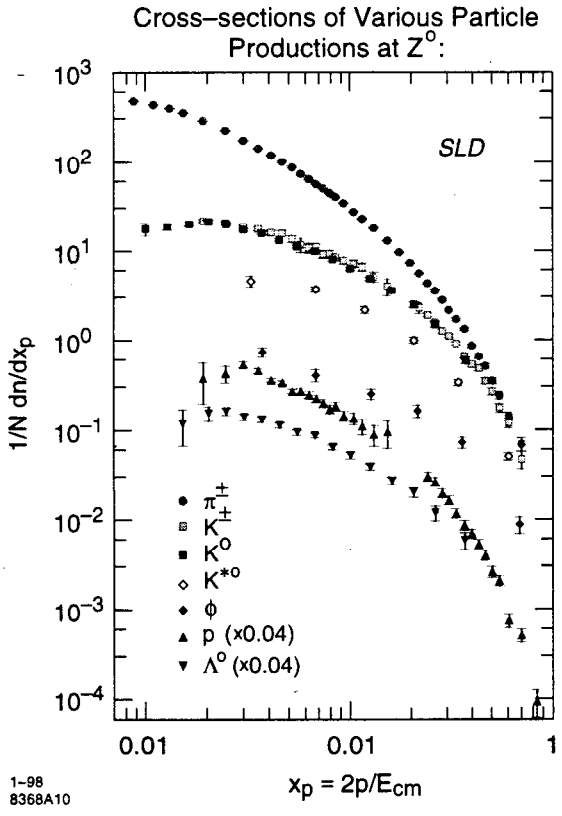

Figure 22. Cross sections for the production of various particle types at the Z^0 [23].

The most important fact is that the CRID contributes to more than a dozen SLD physics analyses. As an example, Fig. 21 shows the charged hadron fractions from Z^0 decays as a function of momentum. CRID identifies pions between 350 MeV/c and 35 GeV/c, kaons between 750 MeV/c and 35 GeV/c, and protons between 750 MeV/c and 45 GeV/c. Figure 22 shows the cross sections for the production of various particles at the Z^0 as a function of the variable x_p [23]. This graph includes also ϕ and K^{*o} production, for which the CRID particle identification is essential for reduction of background.

IV. INTRODUCTION TO DIRC

The DIRC concept was suggested by B. Ratcliff [24] to perform the particle identification in the BaBar detector at SLAC. Its proof of principle was demonstrated in the test beam [25]. DIRC's main advantage is an apparent operational simplicity. The Cherenkov ring is created in the quartz radiator, propagated along its 5m length, brought through the magnet steel and imaged in a system of ~10,000 photo-multipliers (PM) (1"dia., EMI 9125B). The concept works as long as no significant distortions occur during, as many as 200 of internal reflections. In a way, the DIRC is a fast optical delay line– see Fig. 23.

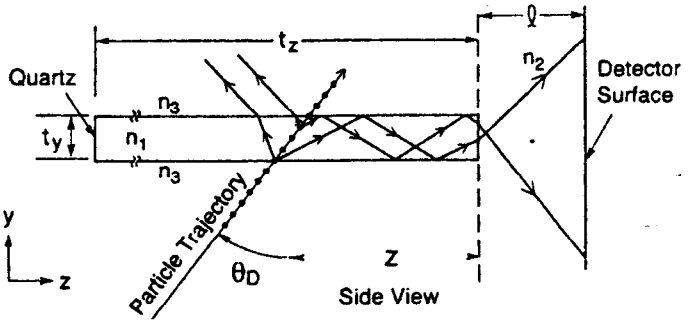

Figure 23. A principle of the DIRC imaging (n_1 and n_2 are refraction indices of quartz and water).

Four quartz bars (1.7cm thick), delivered as 1.2m long segments, are glued to ~5 m length. Fig. 24 shows how twelve such ~5 m long quartz bars are assembled into one bar box. There are 12 bar boxes in the final DIRC – see Fig.25.

There are many challenges associated with the construction of DIRC. The most difficult challenge is to build the quartz radiator, which is mechanically precise (dimensions to ±25μm, squareness to 0.25mrad), and optically good (a transmission >99%/m, an internal reflection coefficient ~0.9995 at 442nm). Another one is a penetration of the magnet steel return with quartz bars; such penetration generates a large stray magnetic field near the PM's of the photon detector. To solve this problem required building a bucking coil and a massive magnetic shield. Another challenge was to build a photon detector with ~10,000 PM's, all submerged in pure water; the water must have a good optical transmission over a distance of one meter.

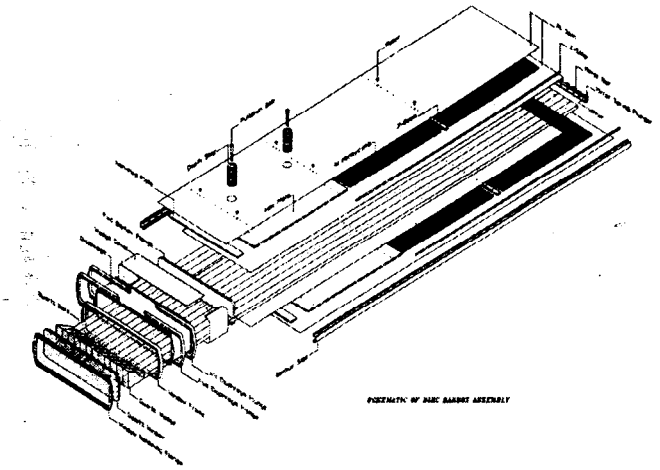

Figure 24. One radiator box with 12 quartz bars, each ~5m long.

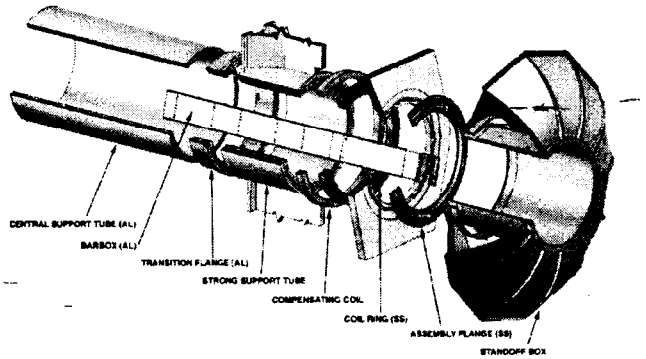

Figure 25. A final engineering layout of the DIRC detector in BaBar, including 12 radiator boxes and the photon detector with ~10,000 photo-multipliers.

J. Simple Estimate of N_o

DIRC photon detector works in visible portion of optical spectrum – see Fig.26. This is necessary to obtain a good optical transmission for a photon propagating through more than 5m of quartz. For example, UV photons needed for the TMAE photo-ionization would not work for the DIRC, i.e., they would be absorbed before reaching the quartz bar end. Therefore, at present, the photo-multipliers are the best choice for such photon detector. Fig. 27 shows a comparison of our transmission data [26] and data from Hereaus Suprasil wet (a large content of OH), which is a fairly good approximation of our Spectrosil 2000 (wet) made by TSL.

The "starting efficiency," is defined, in case of DIRC, by the wavelength dependent transmission through quartz, $T_{quartz}(E)$, the transmission through five joints needed to glue bars together with an optical epoxy EPOTEK 301-2, and the photo-multiplier quantum efficiency, $\varepsilon_{PM}(E)$, which has to be corrected for its window transmission submerged in water. There are many corrections degrading the "starting efficiency." They are derived from a collection of efficiencies, such as those measured during the construction period (transmission of quartz, internal reflection coefficient of quartz bar, mirror reflectivity), and those measured during the run [electronics threshold efficiency (its value is governed by a noise), optical transmission of water], together with estimates of other factors, such as loss of light in various imperfection in the quartz bars (known damages), gaps between bars, bar boxes, etc. We call the degraded efficiency a "final efficiency." The "starting" and "final" efficiencies are shown in Fig. 26, and Table 2 lists present estimates of the total degradation factors between the "starting efficiency" and the "final efficiency."

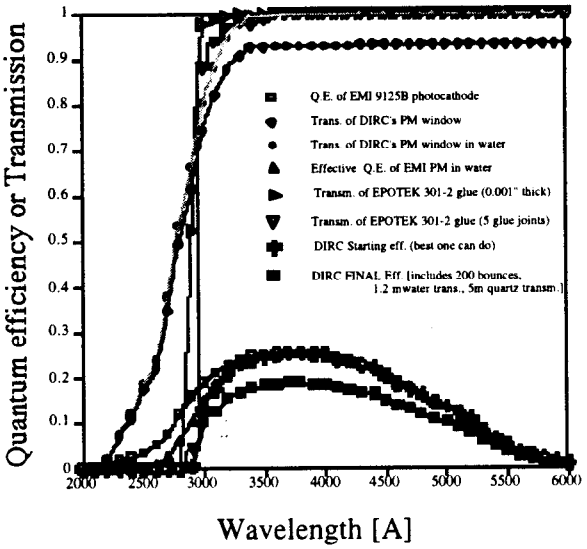

Figure 26. DIRC performance: quantum efficiency of EMI9125B PM, transmission in its window, transmission of its window in water, effective quantum efficiency of PM submerged in water, transmission of 0.001" thick EPOTEK 301-2 optical epoxy, transmission of five glue joints, DIRC starting efficiency, and DIRC final efficiency assuming 200 internal reflections, transmission in 5 m of quartz and transmission in 1.2m long water path.

Fig. 26 shows that the EPOTEK301-2 epoxy plays a similar "transmission cut-off" role in the DIRC as the fluorocarbon radiators did for the CRID, i.e., they define a low wavelength acceptance of the overall detector. Just as CRID had to pay an outmost attention to the fluorocarbon purity, DIRC must make sure that the EPOTEK epoxy does not deteriorate in time due to either a radiation or yellowing due to a large photon dosage.

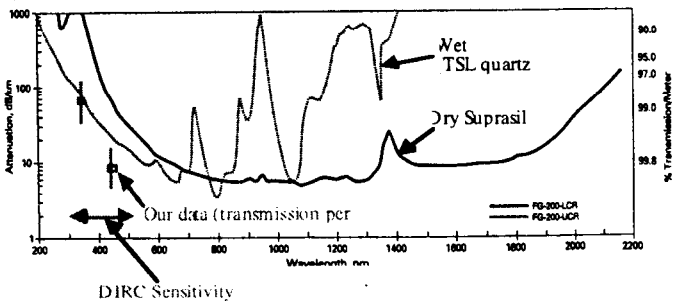

Figure 27. Quartz transmission as a function of photon wavelength for wet and dry Hereaus Suprasil fused silica quartz; DIRC quartz, made by TSL, is expected to perform similarly to wet case (graphs also shows our transmission measurements and the DIRC sensitivity window).

Table 1. DIRC expected final performance.

Parameter	Value
Total fraction of photoelectrons contributing to the "final efficiency" compared to the "starting efficiency" $Eff_{final}/Eff_{starting}$	0.74
Mean photon energy :	3.2eV
Mean refraction index :	1.474
Mean Cherenkov angle (β=1 particle) :	47.3°
Radiator :	quartz
Radiator thickness (0° incidence) :	1.7 cm
N_0	41 cm^{-1}
Expected average number of photoelectrons per full ring (β=1 particle and 25° incidence) :	29

It is clear that the above simple way of calculating the N_0 can be used only as guidance. The performance of DIRC was studied extensively with the Monte Carlo programs. Fig. 28 shows an example of expected pi/K separation in the device.

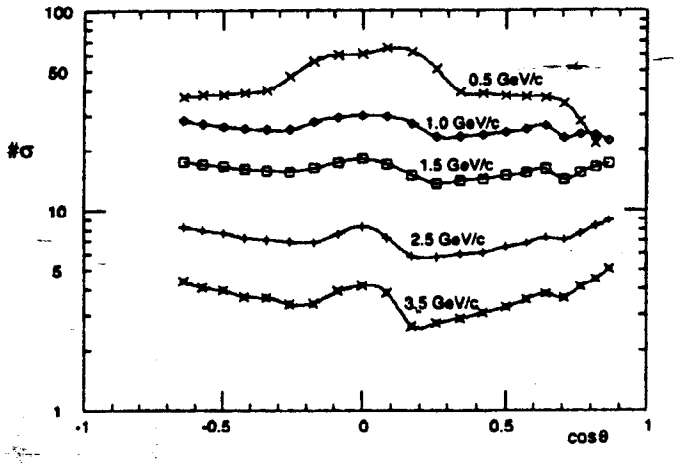

Figure 28. Monte Carlo prediction of DIRC pi/K separation.

K. Some examples from DIRC R&D

As in the CRID's case, any new technique represents many challenges. In the early stages of the DIRC development, these were the following concerns: (a) quartz transmission, (b) quartz internal reflection coefficient, (c) surface pollution, (d) radiation damage of quartz and optical glues, (e) optical glue yellowing under a large photon flux, (f) water purity, (h) water leaks, (i) water corrosive characteristics, (g) quartz mechanical dimensions, (k) background, etc.

It is already clear that some initial worries were justified. At this point, we had to deal with the following issues: (a) natural quartz radiation sensitivity, (b) optical distortion in synthetic quartz, and (c) difficulties associated with the bar production. For example, Fig. 29(a) illustrates that the natural quartz would be a poor choice for DIRC at BaBar, because its radiation hardness is poor [27, 28]. Instead, it is necessary to choose the synthetic quartz – see Fig. 29(b). The synthetic quartz impurity content is generally between 10^3 to 10^6 better that that of the natural quartz.

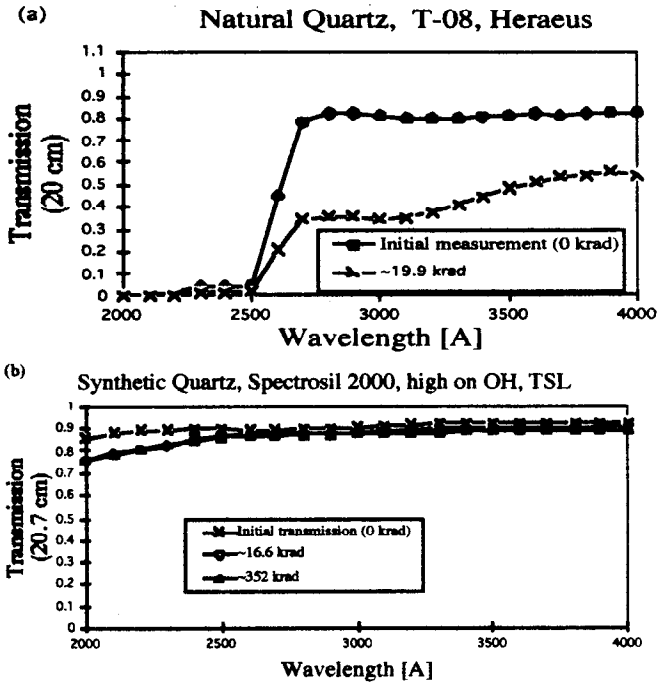

Figure 29. Radiation damage sensitivity of (a) natural quartz T-08 made by Hereaus, and (b) synthetic quartz Spectrosil 2000 made by TSL.

Transmission of various optical glues was also carefully investigated – see Fig. 30. At the end, the choice of hard optical epoxy EPOTEK 301-2 was preferred because the RTV glues do not have a sufficient strength, and the EPOTEK epoxy radiation hardness is sufficient for the BaBar – see Fig. 31.

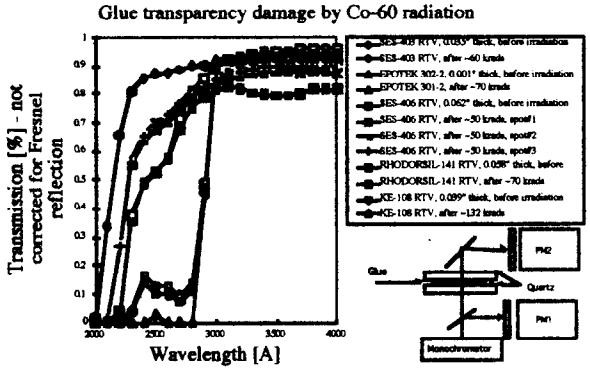

Figure 30. Transmission of various optical glue candidates.

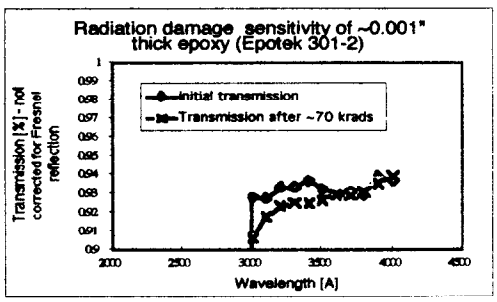

Figure 31. Radiation damage sensitivity of EPOTEK-301-2 epoxy.

DIRC relies on a stability of the internal reflection coefficient (a photon could see as many as 200 bounces). Its value is controlled by a quartz surface finish, and by a surface pollution. We have developed a measuring technique of this coefficient [27], which we call the calorimetric method – see Fig. 32(a). Fig. 32(b) shows the measurement of (1-reflection coeff.) as a function of wavelength [29]. We can see that the data supports the surface rms finish of ~10Å, assuming a pollution-free surface (the manufactures now claims thatit delivers ~5-6Å surface finish).

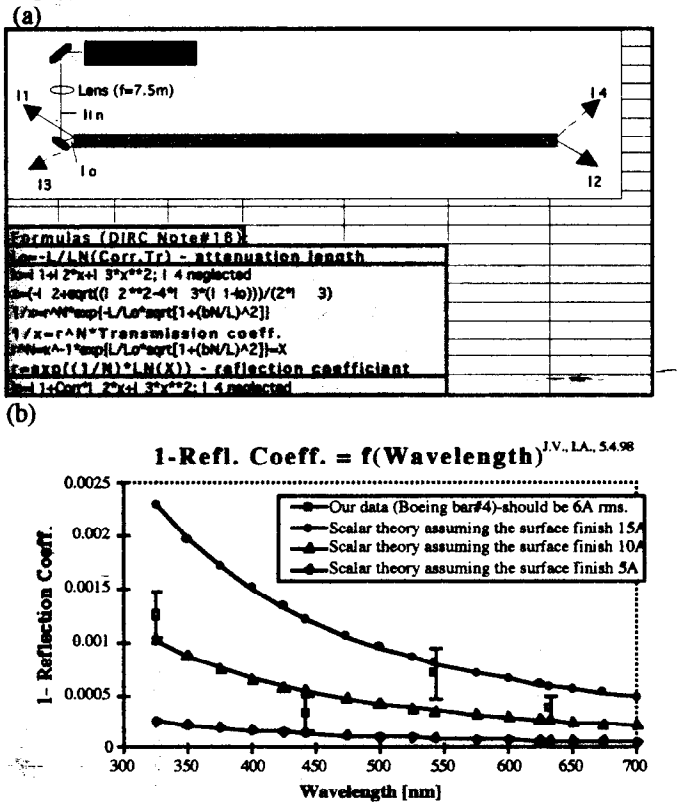

Figure 32. (a) A concept of measuring method to determine the internal reflection coefficient of DIRC bars, (b) a comparison of our measurements and the scalar scattering theory assuming only surface randomness (data are consistent with <10Å rms surface finish).

One consequence of switching from the natural quartz to the synthetic quartz, which is manufactured in a pole shape for DIRC, was a discovery that the quartz is deposited in layers as depicted in Fig. 33(a). This creates a slight modulation of the refraction index [30, 31], which can result in an observation of "shadow-light pattern," if the quartz is properly aligned (a similar effect is observed in a well maintained forest) – see Fig. 33(b). One also obtains a diffraction if one sends a laser light at appropriate angle. Different quartz sources show a different degree of this effect: (a) we see no effect in the quartz used for the CRID liquid radiators (made by Dow Corning), a large and non-tolerable effect in the Suprasil quartz made by Hereaus, and a small and tolerable effect in Spectrosil 2000 quartz made by TSL. The TSL quartz was selected for DIRC because of this measurement result.

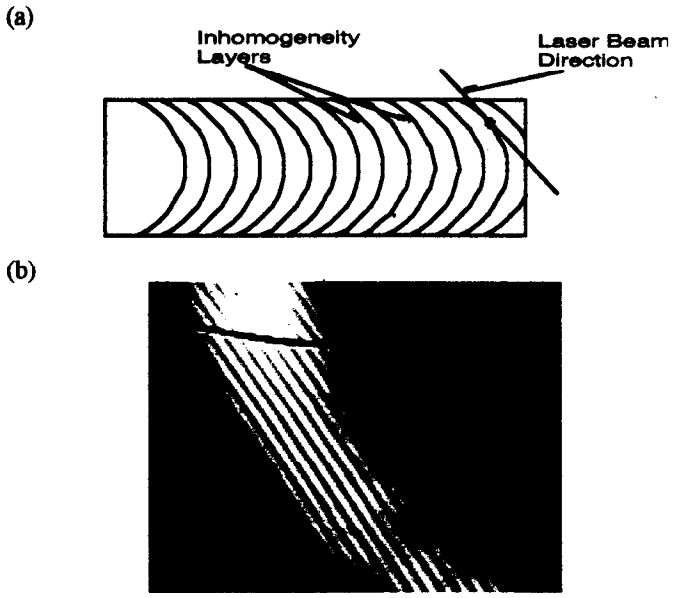

Figure 33. The SiO_2 is deposited in layers in this particular synthetic quartz which modulates the value of the refraction index: (a) ingot and layers, (b) a microscope picture of a bar inclined at certain angle using a halogen light.

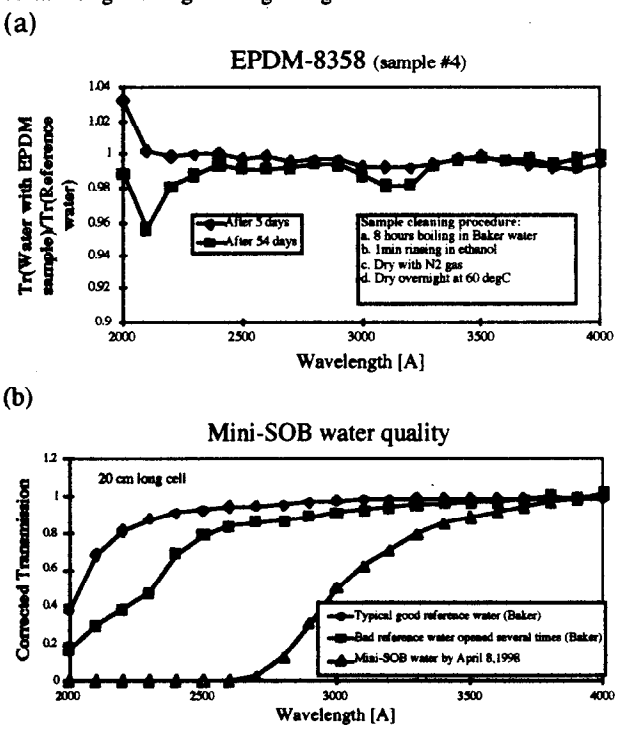

Figure 34. DIRC water transmission in 20cm long cell: (a) with a sample of EPDM gasket used to seal the bar boxes, (b) effect of water stagnation.

The purity of the water represents also a challenge, because DIRC requires a good water transmission over a distance of one meter. One should be careful with the material choices. For example, Fig. 34(a) shows a transmission measurement through 20cm of water contaminated by the EPDM flexing material [32], which is needed to couple the bar boxes to the magnet steel. When treated appropriately (boiling in clean water), the EPDM material is acceptable to DIRC. Fig. 34(b)

shows the effect of water stagnation. Similar result was reported in Ref.33. It is necessary to circulate the water through DIRC and remove the impurities with filters. Similarly, one has to treat water for bacteria growth, etc.

Another important issue is the quartz surface pollution generated by the gas system components, various glues, etc. We have a long term laser test monitoring the internal reflection coefficient as a function of various pollution sources. So far, we have found that it is reasonable independent of this phenomenon in the DIRC wavelength region [33].

Finally, last but not the least, there is an issue of the quartz dimensions. We have constructed a digital microscope, which proved to be an invaluable tool to investigate the bar squareness and edge quality [34]. This work is in progress.

VI. CONCLUSIONS

A major achievement of the first generation photon detectors, such as the CRID, was to convince the many skeptics in the high energy physics community that the RICH concept can be implemented to yield useful physics. The members of the SLD collaboration are "embracing" the CRID as an important tool in a wide range of physics analyses.

The DIRC is a continuation of this effort in the area of the Cherenkov Ring Imaging. Although it is yet to be proven as a viable particle identification concept in a real experiment, its main attraction - a possible operational simplicity, is sufficiently strong argument to pursue this concept, despite of the engineering difficulties to produce the bars of sufficient precision at present.

VII. REFERENCES

[1] J. Sequinot and T. Ypsilantis, "Photo-ionization and Cherenkov ring imaging," *Nucl. Instr. Methods*, 142 (1977) 377.

[2] DELPHI Proposal, LEPC 83-3 and LEPC 84-16, and "The ring imaging Cherenkov detector of DELPHI," *Nucl. Instr. Methods*, A343 (1994) 68.

[3] D.W.G.S. Leith, "Status of Cherenkov ring imaging systems," *Nucl. Instr. Methods*, A265 (1988) 120.

[4] K. Abe et al., "Electrostatic design of the barrel CRID and associated measurements," *Fifth International Conference on Instrumentation for Colliding Beam Physics*, Novosibirsk, Russia, March 15, 1990.

[5] K. Abe et al., "Performance of the CRID at SLD," Nucl. *Instr. Methods*, A343 (1994) 74.

[6] K. Abe et al., "Production of 400 mirrors with high VUV reflectivity for use in the SLD Cherenkov ring imaging detector," *Nucl. Instr. Methods*, A300 (1991) 501.

[7] J. Va'vra, "How many photoelectrons we expect in the Barrel CRID based on the hardware considerations?," *CRID Note* 89, January 1997, including addendum to it.

[8] D. Aston et al., "Development of the SLD single-electron wire detector," Nucl. *Instr. Methods*, A283 (1989) 590.

[9] F. Suekane and Y. Iwasaki, *CRID Note* #79, March 24, 1993.

[10] J. Va'vra, "Wire aging of hydrocarbon gases with TMAE additions," *IEEE Trans. Nucl. Sci.*, NS-34, p. 486, Feb. 1987; "Review of TMAE wire aging in CRID detectors," *CRID Note* #36, SLAC (1987); and "Construction and initial operation of a proportional wire detector for use in a Cherenkov ring imaging system," *IEEE Trans. Nucl. Sci.*, NS-35, pp. 487, Feb. 1988.

[11] J. Va'vra, "Can TMAE photocathode be used for high rate applications?," *Nucl. Instr. Methods*, A367 (1995) 353.

[12] E. Spencer et al., *IEEE Trans. Nucl. Sci.*, NS-35, p. 231, Feb. 1988; P. Antilogus et al., "Cherenkov ring imaging detector front-end electronics,"SLAC-PUB-5120, Oct. 1990; K. Abe et al., "Performance of the front-end electronics and data acquisition system for the SLD Cherenkov ring imaging detector," SLAC-PUB-5679, Nov. 1991.

[13] P. Rensing, Ph.D. thesis, SLAC Report 421, Aug. 1993.

[14] D. Anderson, "A photo-ionization detector for the detection of Xenon light," *IEEE Trans. Nucl. Sci.*, NS-28, p. 842, Feb. 1981.

[15] R.T. Rewick, T. Weber, M. Cavalli-Sforza, M.L. Schumacher, and S. Shapiro, "Tetrakis-(dimethylamino)-ethylene: analysis and compatibility with common laboratory materials," *Anal. Chem.* 60 (1989) 2095.

[16] M. Cavalli-Sforza, *CRID Note* 15, May 1986.

[17] G. Lenzen, private communication and E. Schyns, Ph.D. thesis, WUB-DIS-96-22, Wuppertal, Germany, 1997.

[18] G. Hallewell et al.,"A sonar-based technique for the ratiometric determination of binary gas mixtures," *Nucl. Instr. Methods*, A264 (1988) 219.

[19] S. Ilie and G. Lenzen, "Perfluorocarbon liquid; specified chemical aspects for the use within the DELPHI RICH," DELPHI 93-33 RICH 54.

[20] P. Antilogus et al., "Monitor and control systems for the SLD Cherenkov ring imaging detector," *Nucl. Instr. Methods*, A293 (1990) 136.

[21] T. J. Pavel, Ph.D. Thesis, SLAC Report 491, Aug.1997.

[22] R.A. Holroyd, J.M. Preses, C.L. Woody, and R.A. Johnson, "Measurement of the absorption length and absolute quantum efficiency of TMAE and TEA from threshold to 120nm," *Nucl. Instr. Methods*, A261 (1987) 446.

[23] D. Aston, D. Muller and T. Pavel, *SLD Physics Note* 58, November 1996.

[24] B. Ratcliff, SLAC-PUB-6047, 1993.

[25] R. Alexan et al., *Nucl. Instr. Methods*, A397 (1997) 261.

[26] J. Schwiening, *DIRC note* #82, September 1997.

[27] H. Krueger, M. Schneider, R. Reif, J. Va'vra, *DIRC note* #18, Jan. 5, 1996.

[28] X. Sarazin, M. Schneider, J. Schwiening, R. Reif and J. Va'vra, *DIRC note* #39, Oct. 15, 1996.

[29] J. Va'vra and I. Adams, "Surface reflectivity as a function of wavelength," *DIRC note* #107, August 1998.

[30] M. Convery, B. Ratcliff, J. Schwiening and J. Va'vra, *DIRC note*#87, September 1997.

[31] I. Adam et al., *IEEE Trans. Nucl. Sci.*, NS-45, p. 450, June 1997.

[32] J. Va'vra and M. Schneider, "Water transmission study for DIRC,"*DIRC note* #55, August 1998.

[33] P. Ageron, P. Besson, P. Bourgeois, *DIRC note* #78, March 1997.

[33] J. Cohen-Tanugi, J. Schwiening and J. Va'vra, "Study of the internal reflection coefficient as a function of the quartz surface pollution," *DIRC note* #108, August 1998.

[34] J. Cohen-Tanugi, M. Convery, M. McCulloch, R. Reif, J. Schwiening and J. Va'vra, "Development of a digital microscope for DIRC," *DIRC note* #109, August 1998.